International Conference on Space Optics—ICSO 2022

Dubrovnik, Croatia

3–7 October 2022

Edited by Kyriaki Minoglou, Nikos Karafolas, and Bruno Cugny,

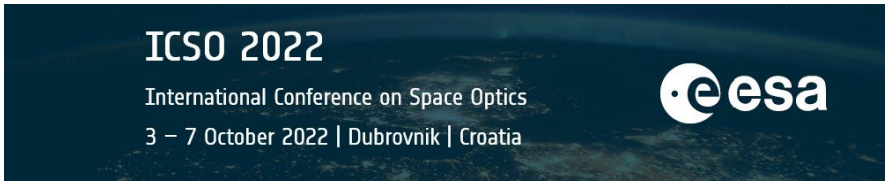

Results of JANUS integration and optical alignment

International Conference on Space Optics — ICSO 2022, edited by Kyriaki Minoglou, Nikos Karafolas, Bruno Cugny, Proc. of SPIE Vol. 12777, 127772O · © 2023 ESA and CNES · 0277-786X · doi: 10.1117/12.2690276

Results of JANUS integration and optical alignment

F. Sarti[a], L. F. Livi[a], A. Galeotti[a], A. Colosimo[a], A. Dattolo[a], I. Ficai Veltroni[a], V. Dalla Corte[b], M. Amoroso[c], L. Agostini[e,f], A. Aboudan[e], and P. Palumbo[d,b]

[a]Leonardo Company SPA, Via delle Officine Galileo 1 - 50013 Campi Bisenzio (Firenze) – Italy
[b]Istituto Nazionale di Astrofisica, Istituto di Astrofisica e Planetologia Spaziali, via Fosso del Cavaliere 100 – 00133 Roma, Italy
[c]Agenzia Spaziale Italiana, Via del Politecnico snc, 00133, Roma, Italy
[d]Università degli Studi di Napoli "Parthenope", Dipartimento di Scienze e Tecnologie, Centro Direzionale Is.C4, 80143 Napoli, Italy
[e]Center of Studies and Activities for Space, CISAS, G. Colombo, University of Padova, 35131 Padova, Italy
[f]INAF - Astronomical Observatory of Padova, Vicolo Dell'Osservatorio 5, 35122 Padova, Italy

ABSTRACT

JANUS (Jovis Amorum Ac Natorum Undique Scrutator) is a high-resolution camera operating in the spectral range 340-1080 nm and designed for the ESA space mission JUICE[1] (Jupiter Icy moons Explorer) planned for launch in 2023 and arrival at Jupiter in 2031. The main scientific goal of the mission is the detailed investigation of Jupiter and its Galileian moons: after three years in Jupiter orbit and many fly-bys with the icy moons, JUICE will be the first spacecraft to be inserted in orbit around Ganymede in 2032. During the final stage of the mission, JANUS is expected to provide images of the moon surface with ground sampling up to 7.5 m/pixel in both panchromatic and narrow band spectral ranges.

Leonardo Spa is the JANUS prime contractor and is in charge, on behalf of the Italian Space Agency (ASI) and in collaboration with the science team led by Parthenope University and the Italian Institute of Astrophysics (INAF), of developing and integrating the Opto-Mechanical Structure of JANUS Optical Head Unit (OHU). The present paper will discuss the procedure adopted for the integration of the OHU and the results in terms of optical quality of the system in flight conditions. Ensuring a Modulation Transfer Function (MTF) close to the diffraction limit at the Nyquist frequency of 71.4 cy/mm constitutes the main challenge for the telescope integration and sets the maximum acceptable transmitted wavefront error to be at most a few tens of nm over the whole field of view.

Keywords: JANUS, JUICE ESA mission, MTF, Wavefront error, Gravity release, Optical alignment, Space Instrument, High resolution camera

1. INTRODUCTION

The JUICE mission will conduct an in-depth comparative study of Ganymede, Callisto and Europa, and will explore most of the Jovian system and Jupiter itself. JANUS will in particular address all mission science objectives related with imaging at different ground resolution and in selected wavenegth bands in the near-UV to the near-IR range. Its main science objectives are summarized below.

Geology of Ganymede, Callisto, and Europa, with special focus on Ganymede: the detailed investigation of the Galilean satellites, which are believed to harbour subsurface water oceans, is central to elucidating the conditions for habitability of icy worlds in planetary systems in general. The study of the Jupiter system and the possible existence of habitable environments offer the best opportunity for understanding the origins and formation of the gas giants and their satellite systems. JANUS will determine the formation and characteristics

Further author information: (Send correspondence to L. F. Livi)
L. F. Livi: E-mail: lorenzofrancesco.livi@leonardo.com

of cryo-volcanic, tectonic, and impact features, relate them to surface forming processes, constrain global and regional surface ages, and investigate the processes of erosion and deposition. Information on spectral trends will allow defining some general compositional properties of surfaces.

Imaging will also contribute to specific geophysical research topics, like the rotation state (including orientation and stability of spin axis and determination of forced librations), which is linked with the internal structure of the bodies and the presence and characteristics of a sub-surface ocean.

Although the moon Io will be observed from distance, JANUS will also allow three year monitoring of its volcanic activities. Surface changes associated with volcanic activity will be investigated using global-scale monochromatic and colour imaging at resolutions of several tens of km/pxl.

For what concerns the Jovian atmosphere, the three upper-most layers can be investigated via imaging observations using different filters: the upper atmosphere (comprising mesosphere, thermosphere and ionosphere), the stratosphere and the upper troposphere. JANUS will study the troposphere, imaging the active dynamical processes, cloud systems, waves, vortices, and other instabilities, determining cloud structure in discrete features, and detecting lightning. It will observe stratospheric variations due to vigorous water meteorology and disturbances from large vortices, such as the Great Red Spot. I twill also investigate the upper atmosphere by imaging auroral activity and particle precipitation in the form of polar hazes.

Finally, JANUS will deliver data on the other targets within Jupiter system. The small inner satellites (Metis, Adrastea, Thebe and Amalthea) are known to be sources of dust for Jupiter's faint ring system. Jupiter's ring system is key to understanding how faint rings can form from the meteoritic bombardment of satellites and then evolve under a variety of forces and external events. In addition to performing a physical characterization of the entire ring system, JANUS will be able to monitor clumps and asymmetries in the ring, search for small-scale vertical structure and track the temporal evolution of the ring and investigate its dynamics.

High-accuracy astrometric positions and multi-filter photometry of all the known moons can be obtained during the tour of the Jovian system. With the exception of Amalthea, the densities of the inner satellites are essentially unknown but astrometric observations of Metis and Adrastea, for example, would allow determination of their densities giving clues to their origin. Likewise, physical and astrometric observations of the dynamical families of the irregular outer satellites would provide important constraints on their origin and evolution, as well as some bounds on their masses from the mutual perturbations. Disk-integrated lightcurve measurements of the irregular satellites will provide their rotation status and hints to their shape.

Being JANUS a high resolution camera, the OHU MTF represents a major optical design driver and a global $\mathsf{MTF} > 0.15$ (including detector and optics) is required in the pancrhomatic channel (400-900 nm). This requirement, together with the extreme sensitivity of the final optical quality to the enforced deformation of the primary mirror, led to the identification of an integration procedure aimed to induce the minimal possible stress on the telescope optical elements. The integration procedure has been validated step-by-step by means of interferometric tests on a flat mirror representative of the telescope primary mirror. Finally, the telescope alignment has been performed exploiting a double-pass interferometric setup and employing a hexapod to adjust the roto-translational positioning of the secondary mirror in order to minimize the wavefront error. After the integration, the MTF performance has been measured in thermo-vacuum conditions representative of the spacecraft operative scenarios. and an estimation of the instrument optical quality in flight has been evaluated taking into account the expected ground-to-orbit elastic deformation of the opto-mechanical structure.

2. OPTICAL DESIGN AND ARCHITECTURE

Janus is a high-resolution imager whose optical layout is derived from a Ritchey-Chrètien telescope.[2,3] The instrument operates in the visible-NIR spectral bands (340-1080 nm) and guarantees diffraction limited performances on a field of view of 1.72×1.29 degrees. The system optical design features a primary and secondary mirror (respectively M1 and M2 in figure 1 realized in fused silica (Hereus HOQ310) and characterized by a 10^{th} order hyperbolic surface. Both the mirrors have been coated with a protected aluminum coating which assures a reflectivity $> 80\%$ in the whole instrument spectral range. In addition to the protected aluminum coating, the primary mirror also features a conductive coating that is ground-wired to the telescope metallic structure. This additional layer, which reduces the mirror reflectivity to 75% in the UV spectral region, is aimed to avoid

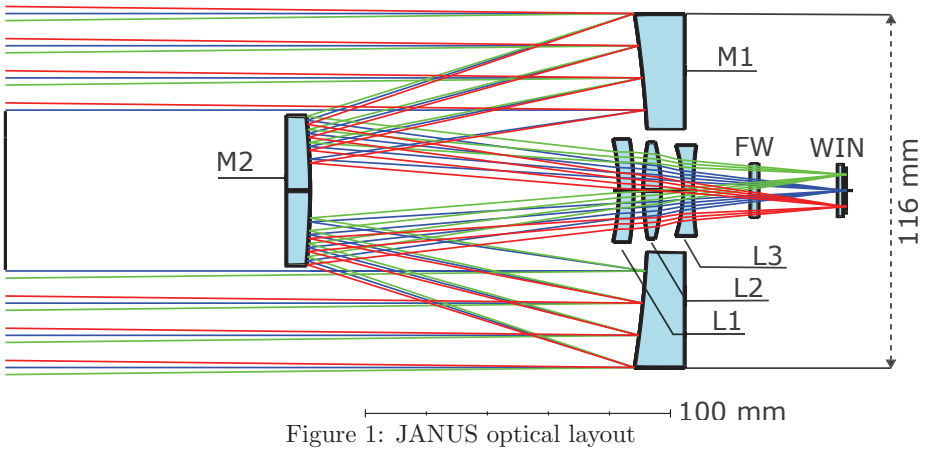

Figure 1: JANUS optical layout

differences of potential between the mirror and the rest of the telescope while the spacecraft crosses the Jupyter magnetosphere's dense plasma environment. The primary mirror, which is characterized by a clear diameter of 116 mm, has an obscuration ratio of 0.45 and acts as the stop of the optical system.

The secondary mirror is followed by a dioptric corrector composed by three spherical elements (L1, L2 and L3 in figure 1), also realized in fused silica. The corrector works with convergent beams and is aimed to suppress in-field residual spherical aberration. In order to maintain apochromatic performances on the whole spectral range, the composite power of the lens triplet is close to zero. The optical layout also includes a filter wheel (provided by IAA-CSIC and SENER) placed between the dioptric corrector and the focal plane. The wheel allows selecting up to 13 different spectral bands (one of which is the panchromatic channel 400-900 nm) accordingly to the mission scientific needs. The filters are made of fused silica and particular care has been devoted to keep the transmitted wavefront error below 100 nm PV in order not to alter the pointing as different filters are selected. The focal plane array (provided by DLR - Institute for Planetary Research, with contribution from CEI - Open University), which is equipped with a fused silica window (WIN in figure 1), completes the optical layout. A list of the main optical properties of the system is reported in table 1. In terms of optical performances, the most critical driver of the design is the instrument MTF which is requested to be at least $\mathsf{MTF}(f_{\mathsf{Nyq}}) = 0.15$ over the whole FOV in the panchromatic spectral range (400-900 nm), where f_{Nyq} is the Nyquist frequency defined as

$$f_{\mathsf{Nyq}} = \frac{1}{2 \times \text{pixel size}} = 71.4 \text{ [cy/mm]} \tag{1}$$

The value of $\mathsf{MTF}(f_{\mathsf{Nyq}})$ takes into account the optical system polychromatic MTF ($\mathsf{MTF}_{\mathsf{OPT}}$) and the detector MTF ($\mathsf{MTF}_{\mathsf{DET}}$) according to the relation

$$\mathsf{MTF}(f_{\mathsf{Nyq}}) = \mathsf{MTF}_{\mathsf{OPT}}(f_{\mathsf{Nyq}}) \times \mathsf{MTF}_{\mathsf{DET}}(f_{\mathsf{Nyq}}) \tag{2}$$

3. OHU THERMO-STRUCTURAL DESIGN

The thermo structural design of the instrument focussed on the combination of materials that would minimise the deformation and the thermal stress during all the phases of the instrument life, but at the same time pursuing the maximum specific stifness, to increase the structural stability of the assembly. The materials selection also aimed at reducing the conductive heat fluxes within the telescope, between the telescope and its surrounding structure and between the instrument and the spacecraft optical bench. For these reasons all the structural elements of the telescope are made of Invar (TCE of $1.3 \times 10^{-6} \mathrm{K}^{-1}$). The mirror supports are connected by means of 3 Invar bars, the distance between the mirrors (and hence the focus position) depends on the thermal expansion/contraction of these bars. Both the telescope and the Filter Wheel Module are mounted on an Invar optical bench (Optical Wall) that defines the mechanical and optical reference for the alignment. The Optical Wall also hosts the Focal

Property	Value
Spectral range	340 to 1080 nm
FOV (2ω)	1.72×1.29 deg
IFOV	15 μrad = 3.09 arcsec
F# without obstruction	4.02
F# with obstruction (radiometric)	4.67
Detector size (Sensitive area)	14×10.5 mm = 2000×1500 pixels (Across track $\times$ Along Track)
Pixel size	7 μm
Pointing stability and knowledge	≤ 8 μrad = 1.65 arcsec

Table 1: JANUS optical performances

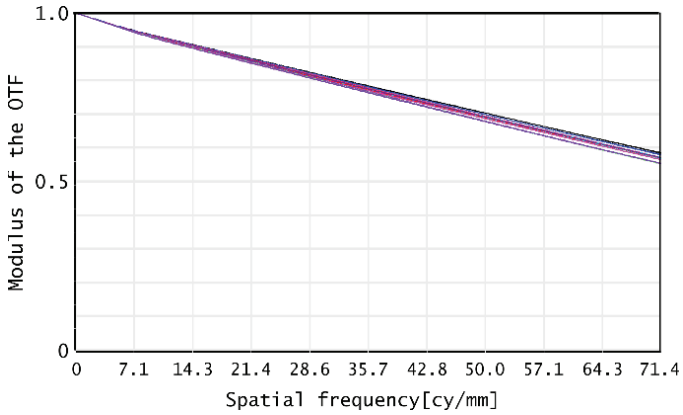

Figure 2: JANUS nominal polychromatic MTF in the spectral range 400-900 nm. The MTF performance results to be close to the diffraction limit for the whole FOV.

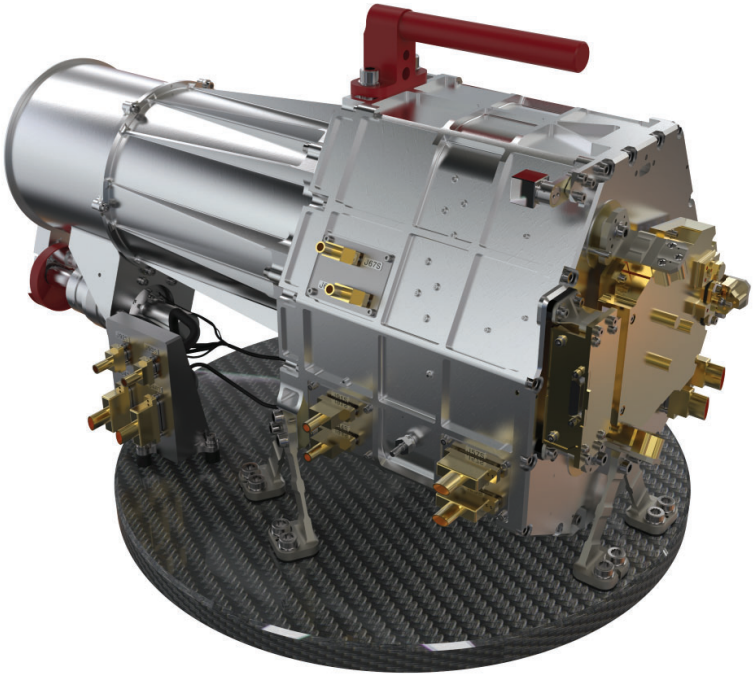

Figure 3: JANUS OHU opto-mechanical assembly.

Plane Module, mounted by means of 3 flexible titanium feet. Attatched to the Optical Wall and evelopping the telescope and the Filter Wheel Module there is an Invar Box (Connecting Wall Structure – CWS), that hosts the electrical interfaces and the thermal control devices (heaters and thermistors). The instrument is conntected to the optical bench of the spacecraft by means of three titanium bipods, ensuring both the thermal isolation from the optical bench and enough flexibility to withstand without damage the high vibration levels experienced during launch. Figure 3 shows a rendered image of the assembly that is completed by an Alluminium baffle and a cover mechanism on top. The whole instrument is covered by Multi Layer Insulation (MLI) in order to thermally protect all its components from the spacecraft and space environment. The thermal control system consists of a set of 'survival' heaters that ensures that the instrument is maintained within a safe non operative

thermal environment regardless of the outer thermal conditions, and a set of 'operational' heaters that target a specific temperature at which the instrument performances are optimised during operational phases.

4. OPTICAL ALIGNMENT PROCEDURE

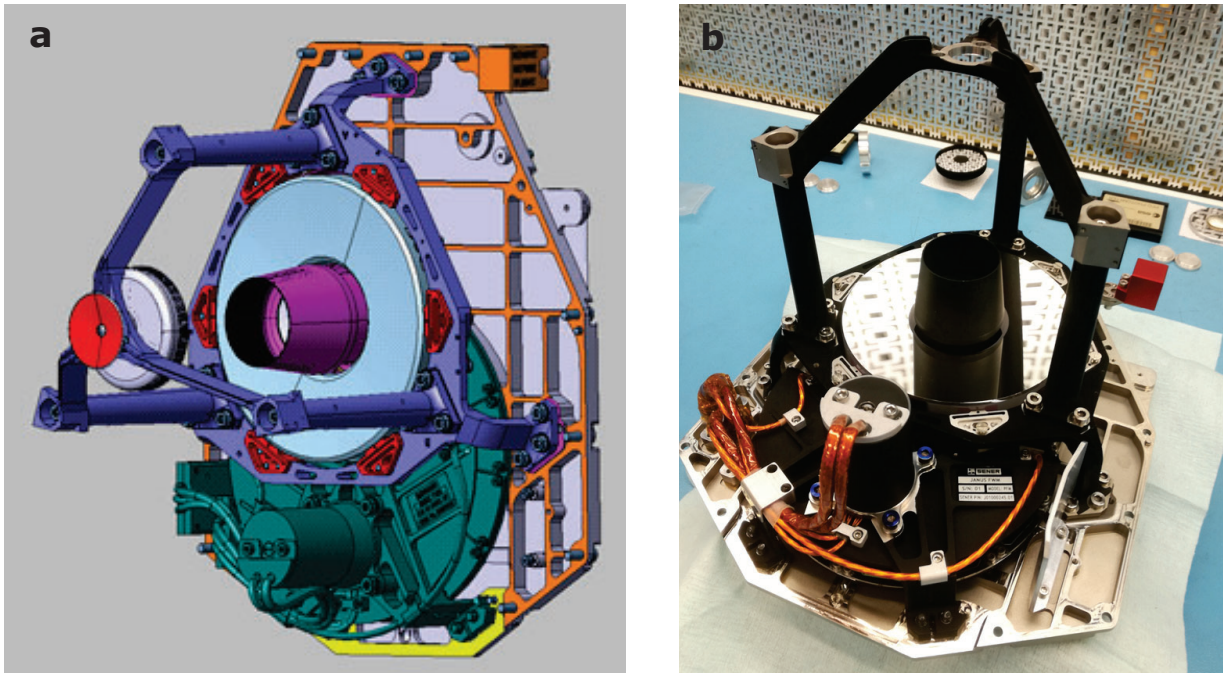

Figure 4: **a:** Telescope structure (violet) placed on the optical bench (Optical Wall) (orange-grey). In red are highlighted the M1 blades, in pink the dioptric corrector and in green the filter wheel module. **b:** Telescope structure with M1, FWM and dioptric corrector already mounted, before the assembly of the external structural box in the intermediate phase of M1 gluing.

The first step in the optical alignment procedure is the positioning of the primary mirror. The primary mirror has been aligned in terms of decentering and tilt with respect to the mechanical optical axis reference frame defined by dedicated reference points on the telescope mechanical structure. A CMM (Coordinate Measuring Machine) has been used for the characterization of the reference frame and a haxapod (Symetrie BORA) has been used for the positioning of the mirror and its holding during the gluing phase. The primary mirror interface consists of six blades (colored in red in figure 4a) secured on the telescope structure by means of three screws and two pins each.

Before proceeding to the mirror integration, the structure has been mechanically and thermally settled in order to stabilize the internal mechanical stress. Additionally, as the adhesive junction is hyperstatic and in order to minimise the distortions induced by the polymerisation of the adhesive, the gluing of the six pads has been performed in two separate steps. In the first step, three of the six blades have been glued after the mirror alignment. At the end of the glue polymerization, the alignment setup has been dismounted and the assembly has been integrated with all the major remaining OHU parts: the dioptric corrector (colored in pink in Figure 4a) has been assembled and the telescope has been installed in its final configuration on the FM optical bench (named Optical Wall, colored in orange-gray in Figure 4a) with the FWM (Figure 4b). Afterwards, the external structural box, the bipods and the inner part of the baffle (see Figure 6a) have been installed. In this configuration, the remaining three M1 blades have been glued and the whole assembly has been cured for polymerisation.

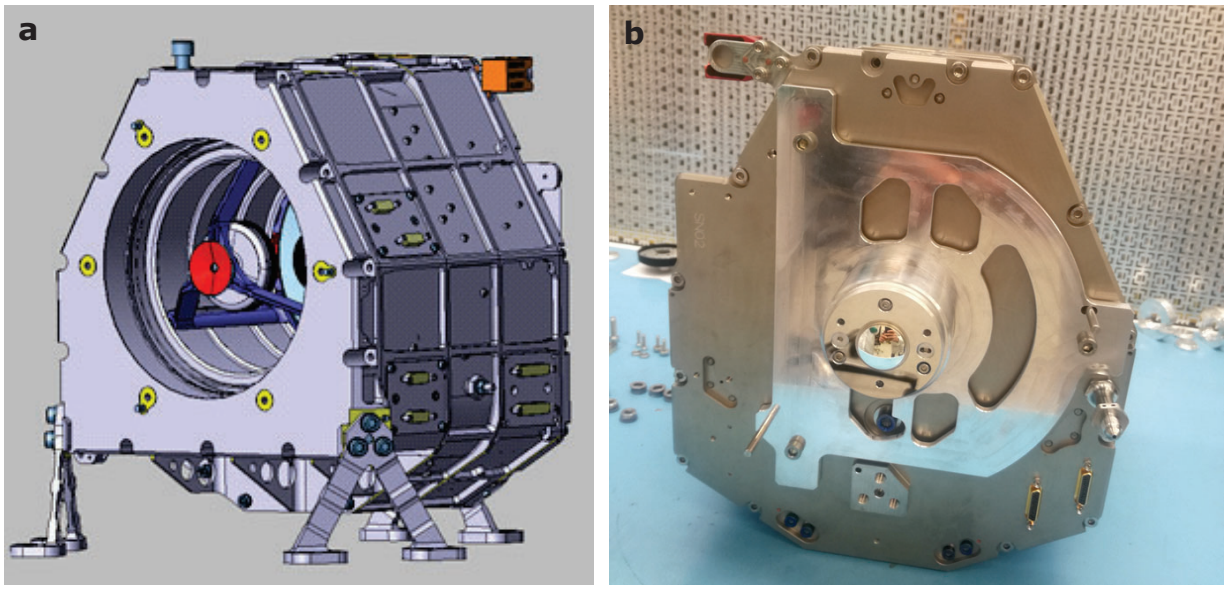

Figure 5: **a:** Assembly configuration for M1 gluing finalization and M2 alignment. **b:** Service sphere used for the definition of FISBA interferometer focus position.

At this point, the only two degrees of freedom remaining in order to recover the instrument optical performance are the positioning of the secondary mirror M2 and of the focal plane array. The alignment procedure of the secondary mirror has been realized exploiting a double-pass interferometric setup and employing a hexapod (Symetrie Bora) and a dedicated service mirror holding system to adjust the roto-translational positioning of the mirror in order to minimize the wavefront error. The test setup consists of a portable *Trioptics FISBA uphase* interferometer operating at 633 nm in convergent beam and a service flat mirror placed in front of the UUT (UUT Unit Under Test) in order reflect back the interferometer light and realize the double pass (see figure 6a). The alignment of the interferometer in the focus of the telescope assembly is performed with the help of a service sphere (6b) that is mounted on the telescope mechanical reference frame interfaces.

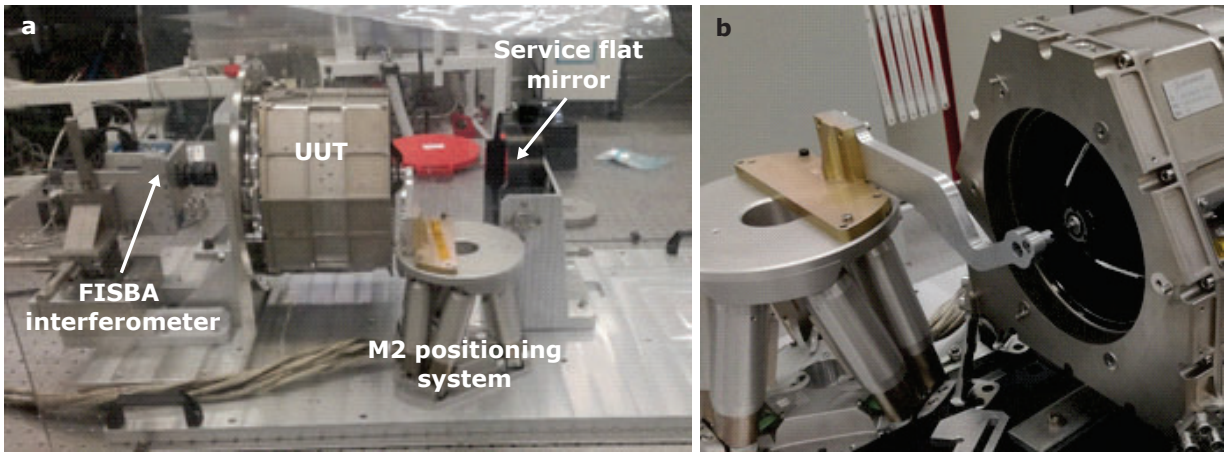

Figure 6: **a:** Double-pass interferometric setup for M2 alignment. **b:** Detail of M2 alignment setup showing the service arm connected to the hexapod holding M2 in position.

The alignment of the reflecting flat mirror is performed using as reference the optical axis of M1. The sphere is then removed and the roto-translational degrees of freedom of the hexapod acting as support for M2 are adjusted in order to recover the best optical quality. For the FOV aligned with M1 optical axis, a mispositioning of M2 results in an aberrated WFE dominated by coma. The mirror alignment is performed exploiting a two-step procedure in which iteratively:

- The coma is zeroed adjusting the x-y translational degree of freedom of M2;
- The pointing is recovered by adjusting the rotation of the mirror around the x-y axes.

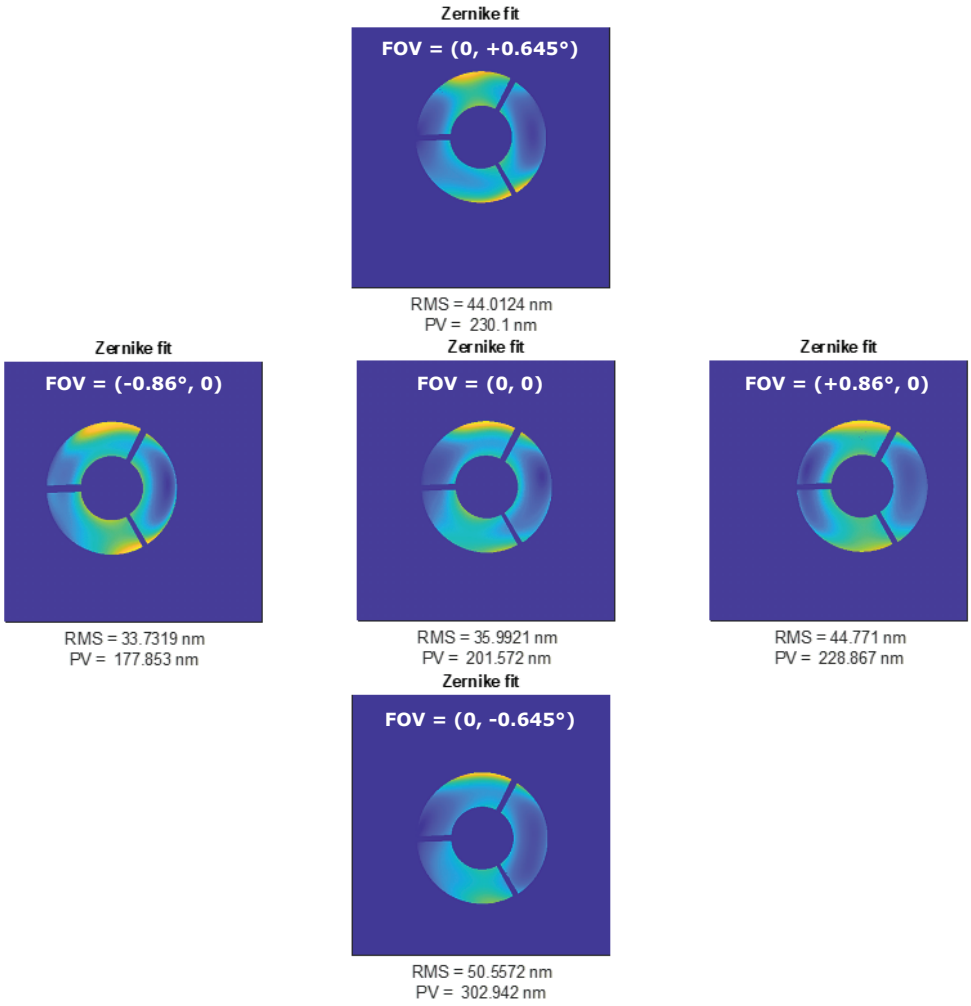

Figure 7: Zernike fit of telescope assembly including M1, M2, dioptric corrector and Filter Wheel Module. .

The amount and typology of aberration is constantly monitored during the mirror alignment by decomposing the WFE on the basis of the annular Zernike polynomials. After the procedure has converged, eventual residual astigmatic aberration is to be ascribed to enforced deformations of the optical surface of the primary mirror. As confirmed by simulated results, for a RC telescope this alignment procedure should ensure that once the WFE is minimized for the central FOV cancelling the coma, no additional adjustment is needed for the off axis fields of view. This is true as long as the folding mirror is perfectly aligned with the instrument optical axis. On the contrary, a residual tilt of the folding mirror results in a non-vanishing astigmatism for the off axis FOVs. This

fictious aberrational content can be minimized by adjusting the tilt of the folding mirror and the FISBA focus position but leaving the secondary mirror unchanged. After this procedure we end up with a WFE characterized by a RMS value in the range between 34 nm and 51 nm on the whole FOV and a aberrational content dominated by a residual astigmatic aberration, as it is shown in figure 7 and in table 2.

FIELD	X [deg]	Y [deg]	AST X [waves]	AST Y [waves]	COMA X [waves]	COMA Y [waves]	SPH [waves]	RMS [nm]
Axis	0	0	-0.01	-0.05	-0.009	0.008	0.02	36
Max X	+0.86	0	-0.002	-0.06	-0.006	0.014	0.02	45
Min X	-0.86	0	0.009	-0.04	-0.008	0.01	0.02	34
Max Y	0	+0.645	0.015	-0.06	0.007	0.008	0.02	44
Min Y	0	-0.645	-0.015	-0.07	-0.018	0.011	0.02	51

Table 2: Measured aberration for different FOV points after alignment and mechanical stress tests.

5. DETECTOR POSITIONING

Once the secondary mirror has been glued in position, the instrument alignment terminates with the positioning of the focal plane array (FPA) module. The quality of the FPA alignment is evaluated in terms of the MTF of the overall system (telescope and detector) by means of the slanted edge method[4,5] and measuring the MTF performance at the Nyquist frequency $f_{Nyq} = 71.4$ cy/mm as the defocus is changed. This measurements exploits a target slit positioned on the focal plane of our OGSE collimator as it is shown in figure 8a. MTF scans through focus are obtained by moving the target slit position along the OGSE optical axis with the slit orientation set along the columns or along the rows of the detector in order to acquire tangential or sagittal MTF curves.

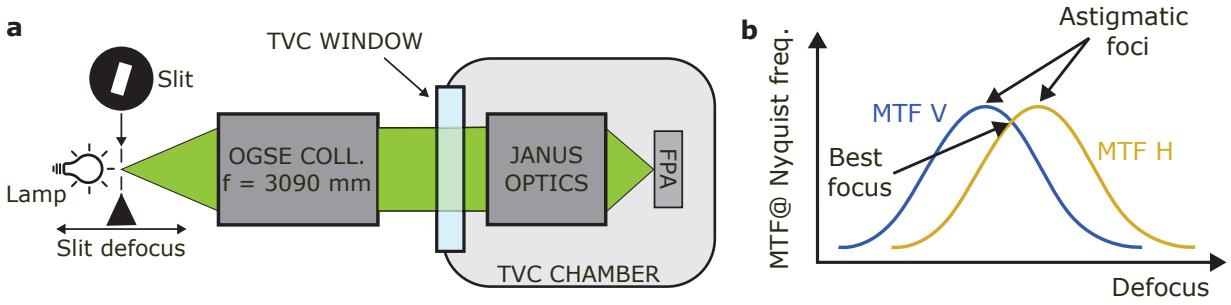

Figure 8: **a:** Schematic representation of slanted edge MTF measurement setup. The slit is positioned in the focal plane of the OGSE and is uniformly illuminated by means of a small integrating sphere coupled with a halogen lamp. The orientation of the slit is optimized in order to result tilted with respect to the rows or the column of the instrument detector of about 5 degrees. **b:** The colored curves report the MTF H and V values at Nyquist frequency at different slit defocusing position. The separation of the two curves is due to the astigmatic aberration of the optical system.

Being the WFE dominated by astigmatism, we expect the sagittal and tangential MTF curves to show two equal-height but separated maxima corresponding to the two astigmatic foci, as it is shown in figure 8b. The midpoint between the two foci corresponds to the non-aberrated focal plane position and represents the position where the focal plane has to be placed in order to obtain the best optical performance on both the directions. This consideration remains true as long as the WFE is dominated by pure astigmatism, independently from the magnitude and orientation of the aberration. As a consequence of this, the eventual astigmatic aberration of the alignment setup will not affect the best focus position, since the sum of two astigmatic aberrations remains an astigmatism.

A first alignment of the FPA has been performed at room temperature in air. The position found at room temperature has then to be properly shimmed in order to take into account the structural thermal deformation

expected passing from the alignment conditions (T = 22 °C) to flight conditions where the instrument will operate in a temperature range between -17 and -31 °C for M1 and M2. Due to the slight difference between the TCE of the optical elements, which are made of fused silica ($\mathsf{TCE} = 0.27 \times 10^{-6}\mathrm{K}^{-1}$) and the telescope structure, which is made of Invar36 ($\mathsf{TCE} = 1.3 \times 10^{-6}\mathrm{K}^{-1}$), the position of the instrument focal plane is expected to increase its distance from the primary mirror as the telescope is cooled down. In particular, we predict that a temperature change from T_{amb} = 22 °C to T_{flight} = -28 °C (middle operative temperature) determines a focal plane displacement of the order of 50 μm which is to be ascribed almost completely to the variation of the mirror radius of curvature and the contraction of the invar structure being the dioptric corrector characterized by a power close to zero. This displacement is only marginally compensated by the thermal deformation of the focal plane module itself, which is characterized by an athermalized structure whose deformation, for the temperature change considered above, is of the order of 1 μm.

The position of the best focus at flight temperatures has been determined placing the instrument in a thermo-vacuum chamber (TVC) where operative scenarios are simulated. However, in thermo-vacuum conditions the slanted edge MTF measurement is affected by a series of systematic effects that displace the focus position from its true value. In particular, in our case, the most detrimental contribution is due to the thermal gradient which originates radially on the TV chamber window as a consequence of the cooling down of the inner walls of the TV chamber itself. This thermal radial gradient, which is characterized by the center of the window colder than the edge, is responsible of a lensing effect which pushes the focus in the same direction as the thermo-elastic deformation of the telescope structure. In order to take into account this effect, we characterized it by means of a dedicated test campaign with double-pass interferometric setup and measuring the amount of power as a function of the difference of temperature ΔT_{win} between the center and the edge of the TV chamber window.

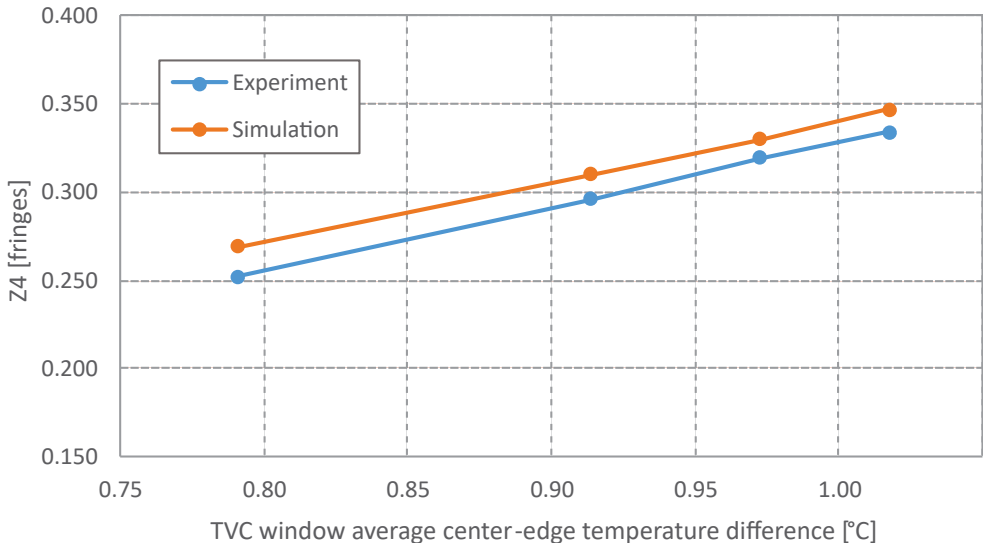

Figure 9: TVC window induced defocus aberration as a function of the average temperature difference between the window's center and edge.

Figure 9 compares the window-induced defocus measured as a function of the temperature difference between the window center and edge with a simulation of the same quantity. The simulation has been carried out with Zemax Optic Studio considering a fused silica window ($n = 1.457$ at 633 nm, radius $R = 75$ mm) characterized by a radial parabolic refraction index gradient $\Delta n(r) = \delta_n(T) \times r^2$ where $\delta_n(T)$ at the first order in the temperature T is given by[6]

$$\delta_n(\Delta T) = \frac{1}{r^2}\frac{n^2-1}{2n} D_0\, \Delta T \tag{3}$$

where $D_0 = 2.24\times10^{-5}$ for fused silica. In particular, at the temperature chosen for the FPA alignment (-28 °C) we measured ΔT_{win}=1.3 °C and the window-induced power resulted to be 0.43 fringes (at 633 nm) which

translates in a focus shift of $\delta_{win} = 42$ um. Another potential source of an apparent focal plane shift is the air-vacuum transition that induces an elastic deformation on the TV chamber window. However, in our case, the 5 cm thickness of the chamber window prevents this effect to play any significant contribution and no variation of power has been detected interferometrically as the pressure inside the chamber is lowered.

In order to separate the defocus induced by the instrument thermal contraction and the apparent effect due to the lensing effect of the TVC window, the best focus position has been evaluated for several operative conditions while keeping constant the thermal gradient on the window. As it is shown in table 3, once the effect of the window has been removed, the experimental focus shift due to the thermal deformation of the telescope shows an excellent agreement with the theoretical value that we determined by means of a model that takes into account:

- The M1-M2 distance contraction and the M1-detector distance contraction, evaluated with FEM analysis;
- The change in radius of curvature and index of refraction of the optical elements, evaluated with Zemax.

	T_{M1}	T_{M2}	$\Delta(M_1 - M_2$	$\Delta(M_1 - DET)$	Defocus Theory	Defocus Experim.
	[°C]	[°C[	[μm]	[μm]	[μm]	[μm]
Performance COLD	-30	-31	-8.9	-7.6	-61	-61
Performance MIDDLE	-24	-25	-7.8	-6.6	-55	-56
Performance HOT	-16.6	-17.6	-6.5	-5.1	-45	-45.5
Room temperature	22	22	0	0	0	0

Table 3: FPA defocus at different operative conditions of the JANUS telescope. Values are reported with respect to aligment conditions at room temperature. $\Delta(M_1 - M_2)$ and $\Delta(M_1 - DET)$ represent respectively the thermal contraction of the mirrors interdistance and the thermal contraction of the M1-detector interdistance.

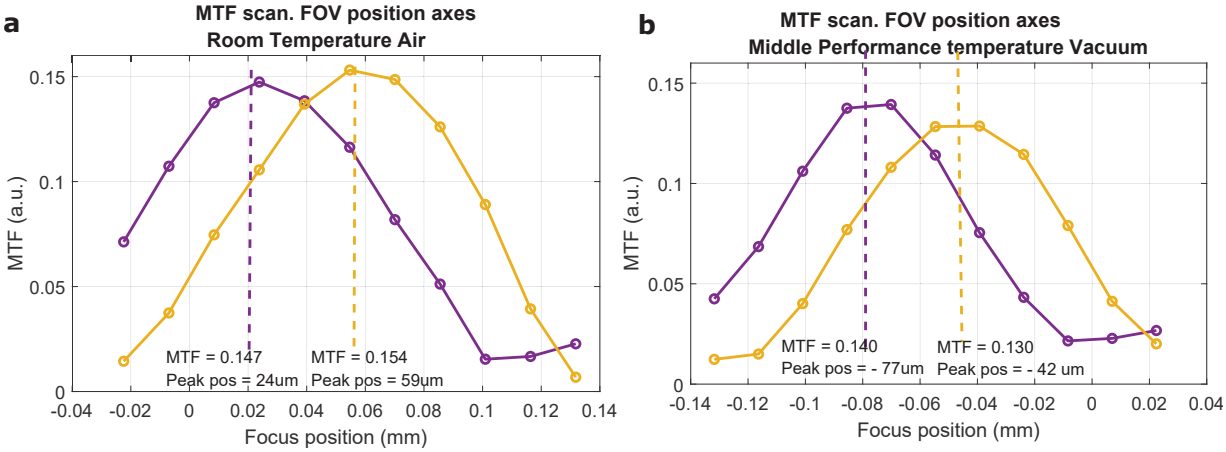

Figure 10: Horizontal and vertical MTF values @ Nyquist frequency wrt detector focus position measured on axis at room temperature (22 °C) (**a**) and operative middle temperature (-28 °C) (**b**). Zero coordinate correspond to expected position at operative temperature. The measured focus position is +42 μm at room temperature and -58 μm at operative temperature, with respectively +42 μm and +56 μm for the average values on the whole FOV. The 100 μ shift between the two focal position is the sum of the effects given by the thermoelastic deformation of the telescope and the lensing effect of the TVC window.

In conclusion, for the middle operative temperature of -28 °C, we end up with two contribution for the shift of the focus position: the first, due to the thermoelastic deformation of the telescope structure is predicted to account a shift of 61 μm; the second, due to the thermal gradient on the TV chamber window, is predicted to

contribute for an additional shift of 42 μm, for a total shift of 102 μm. This shift matches the one measured experimentally considering the accuracy error, as it is shown in figure 10 where the MTF measured for the field in-axis in air at 22 °C is compared to the one measured in TV conditions at -28 °C obtaining an average shift value of 98 μm.

6. INSTRUMENT MTF PERFORMANCES

The estimation of the absolute MTF value of JANUS camera it's a very challenging activity. As a matter of fact, in order to predict the flight MTF value at the focus position, the MTF value obtained with the slanted edge method described in section 5 must be purged of several contributions that are not negligible at the Nyquist frequency. The contributions considered in the analysis are:

- the OGSE collimator transmitted wavefront error which is comparable to the aberrational content of the telescope. The OGSE contribution will be described in section 6.1.
- the elastic deformation of the primary mirror surface due to the the gravity release. This effect is described in section 6.2.
- the difference between the emission spectrum of the lamp used to perform the measurement and the spectrum of the science scenario. This contribution is described in section 6.3

All these contribution have been removed by analysis with the procedure described in section 6.4.

6.1 OGSE contribution

The OGSE used for testing JANUS presents a WFE of about 30 nm RMS on the dimension of JANUS pupil (116 mm). Considering that JANUS optical quality is very close to the diffraction limit, with values of WFE between 34 and 51 nm RMS, the OGSE WFE aberration cannot be considered negligible. The OGSE WFE has been characterized both at ambient conditions and in TVC conditions by exploiting a double pass interferometric measurement. The measurement has been performed by placing a TRIOPTICS FISBA interferometer at the focal point of the collimator and a thick flat service mirror inside the TVC chamber. This setup allows to evaluate both the WFE contribution of the OGSE collimator and of the TVC chamber window.

6.2 Gravity release contribution

The gravity release affects the optical elements of the instrument by altering their interdistances and deforming the the optical surfaces. From our analysis it comes out that the dominant contribution affecting the optical performances derives from the deformation of the primary mirror optical surface under the effect of its own weight. This effect has been simulated by means of a FEM analysis and the deformed sag has been imported on Zemax Optic Studio where its evaluation in terms of Zernike polynomials has been carried out. In particular, the analysis predicts that, because of the gravity release, the astigmatic contribution to the wavefront error should be modified by increasing the Zernike coefficient C_6 by 0.22 annular fringes. This result has been confirmed experimentally with an double-pass interferometric measurement during preliminary tests performed on the optical engineering model. The interferometric tests exploit the scheme already described in section 4 and the instrument WFE has been acquired with the telescope placed in two different geometrical arrangements, the first being the "normal" arrangement and the second by rotating the instrument (and the FISBA interferometer) by 90 degrees. The 90 degrees rotation makes the weight force acting along the vertical axis to vanish, allowing a "0g" test of performance on that axis. As it is shown in figure 11. the measurement revealed a variation of 0.216 annular fringes for the Zernike coefficient C_6, a variation that is in excellent agreement with the FEM predicted value.

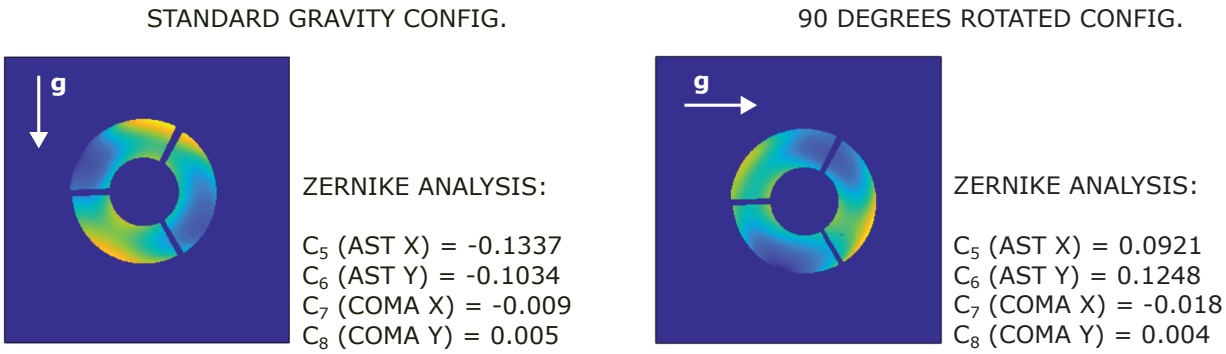

Figure 11: Interferometric measuerement of JANUS transmitted wavefront error in the standard configuration (left) and in the configuration with the instrument rotated by 90 degrees (right). In the instrument coordinate reference frame, gravity acts along different directions in the two measurements. This affects the deformation of the primary mirror optical surface due to its on weight and this effect is captured by the Zernike analysis which reveals a difference of about 0.22 annular fringes for both the astigmatic coefficients in the two cases.

6.3 Spectrum contribution

The final step in order to obtain the MTF value purged from all the unwanted contributions is the spectrum correction. As it is shown in figure 12, the expected in flight scenarios presents an average spectrum with very low component in the near infrared region (where the instrument has lower MTF performances) with a peak centered around 500 nm where the in instrument presents a much higher MTF value. On the contrary, the lamp used for testing presents a an opposite spectrum with low intensity in the UV/VIS region and a peak moved to the NIR part. This different spectral distribution strongly affects the final value of the polychromatic MTF in the range 400-1100 nm with a performance expected to decrease as the IR contribution in the spectrum increases.

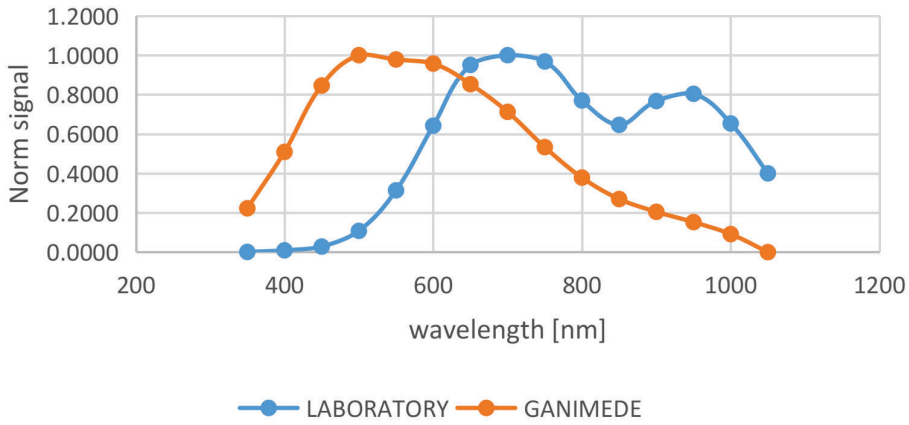

Figure 12: Normalized OGSE test lamp emission spectrum (blue) compared with the Ganimede surface average normalized spectrum (orange).

6.4 MTF estimation procedure

As mentioned above, the estimation of the instrument MTF in flight conditions has been evaluated starting from the slanted edge MTF curves acquired in thermo-vacuum condition and taking into account the OGSE, the gravity release and the spectrum contribution. As a first step, the complete setup (JANUS + OGSE) has been simulated on Zemax Optic Studio and the experimental aberrational contribution of the OGSE has

Temperature case	M1 temp.	Focus position	MTF V	MTF H
Performance COLD	-30 °C	21 μm	15.0 %	14.4 %
Performance MIDDLE	-24 °C	-16 μm	16.1 %	15.9 %
Performance HOT	-16.6 °C	-1 μm	17.3 %	17.3 %

Table 4: In flight estimation of JANUS MTF performance at the Nyquist frequency (71.4 cy/mm) on F1 (PAN) filter (transmission range 400-900 nm) for three different instrument operative conditions.

been inserted as a Zernike phase retard surface. The Zernike terms of an annular phase retard surface which simulates JANUS transmitted wavefront error have then been adjusted in order to reproduce the experimental MTF curves. In this "fit" we assume that JANUS is affected only by astigmatic aberration (an assumption well supported by interferometric measurements), a wavelength-independent detector MTF = 0.30 (spectral average value on detector MTF measurements) and a spectrum given by the convolution of the lab white lamp, the detector quantum efficiency and the OGSE+JANUS transmission in the range 400-900 nm. From the value of this "fit" that reproduces the configuration JANUS + OGSE, we removed the OGSE contribution obtaining the JANUS transmitted wavefront error (WFE). After this step, the MTF is evaluated using the Ganimede spectrum in place of the lamp spectrum. Finally, the gravity release contribution is included by increasing the JANUS astigmatism coefficient C_6 by 0.22 annular fringes and the MTF is evaluated at the focus position corresponding to the various operative temperature cases. Table 4 reports the MTF estimation at the end of the analysis for three different operative scenarios of the instrument.

7. CONCLUSIONS

JANUS high resolution camera alignment and integration method has been driven by the requirement of a $\mathsf{MTF} > 0.15$ in the panchromatic wavelength range and for the whole field of view. Considering the instrument operative temperature, the design volume and mass constraint this has been a complex activity that requested several dedicated design and integration challenging solutions.

The results obtained in terms of optical quality of the instrument are in line with the expected values and compliant with the requirements. The complete system MTF resulted to be > 0.144 for all the operative temperature scenarios and exceed the requested value of 0.15 if the temperature of the system is set to be in the higher part of the operative range. All the reported values have been measured after the instrument qualification test campaign highlighting negligible variations with respect to initial values.

ACKNOWLEDGMENTS

The involvement of Leonardo as JANUS Instrument Prime contractor and OHU design authority is performed in the frame of Italian Space Agency (ASI) Industrial Contract N. 2018-01-I.0. The Italian Principal Investigator team acknowledges support from ASI under ASI-INAF agreement N. 2018-25-HH.0.

We would like to give a special acknowledgement to Andrea Turella, Giovanni Noci and Riccardo Paolinetti for their fundamental contribution to the development, design, test and integration of the instrument.

REFERENCES

[1] Grasset, O., Dougherty, M., Coustenis, A., Bunce, E., Erd, C., Titov, D., Blanc, M., Coates, A., Drossart, P., Fletcher, L., Hussmann, H., Jaumann, R., Krupp, N., Lebreton, J.-P., Prieto-Ballesteros, O., Tortora, P., Tosi, F., and Van Hoolst, T., "Jupiter icy moons explorer (juice): An esa mission to orbit ganymede and to characterise the jupiter system," *Planetary and Space Science* **78**, 1–21 (2013).

[2] Della Corte, V., Noci, G., Turella, A., Paolinetti, R., Zusi, M., Michaelis, H., Soman, M., Debei, S., Castro, J. M., Herranz, M., Amoroso, M., Castronuovo, M., Holland, A., Lara, L. M., Jaumann, R., and Palumbo, P., "Scientific objectives of janus instrument onboard juice mission and key technical solutions for its optical head," in [*2019 IEEE 5th International Workshop on Metrology for AeroSpace (MetroAeroSpace)*], 324–329 (2019).

[3] Turella, A., Corte, V. D., Paolinetti, R., Palumbo, P., Amoroso, M., Castronuovo, M., and Mugnuolo, R., "Structural-Thermal-Optical-Performance (STOP) analysis for the prediction of the line-of-sight stability of JANUS camera on board JUICE ESA mission," in [*Optical Modeling and System Alignment*], Kahan, M. A., Sasián, J., and Youngworth, R. N., eds., **11103**, 101 – 112, International Society for Optics and Photonics, SPIE (2019).

[4] G. Bostan, P. Sterian, T. N. A. B. and Sarafoleanu, C., [*The slanted-edge method application in testing the optical resolution of a vision system*], JOURNAL OF OPTOELECTRONICS AND ADVANCED MATERIALS (2019).

[5] K. Masaoka, T. Yamashita, Y. N. and Sugawara, M., [*Modified slanted-edge method and multidirectional modulation transfer function estimation*], Optics Express (2014).

[6] Bach, H. and Neuroth, N., [*The properties of optical glass*], Springer (1998).